



RESEARCH LETTER

10.1002/2015GL067284

Key Points:

- Pacemaker climate simulations show delayed response of tropical Pacific to tropical AMO
- The delay is linked to subsurface oceanic anomalies in western tropical Pacific
- Seawater salinity is a crucial factor for multidecadal evolution of tropical Pacific Ocean

Supporting Information:

- Supporting Information S1

Correspondence to:

D. Zanchettin,
dave.zanchettin@unive.it

Citation:

Zanchettin, D., O. Bothe, H. F. Graf, N.-E. Omrani, A. Rubino, and J. H. Jungclaus (2016), A decadal delayed response of the tropical Pacific to Atlantic multidecadal variability, *Geophys. Res. Lett.*, 43, 784–792, doi:10.1002/2015GL067284.

Received 3 DEC 2015

Accepted 4 JAN 2016

Accepted article online 7 JAN 2016

Published online 30 JAN 2016

A decadal delayed response of the tropical Pacific to Atlantic multidecadal variability

Daive Zanchettin^{1,2}, Oliver Bothe¹, Hans F. Graf³, Nour-Eddine Omrani^{4,5}, Angelo Rubino², and Johann H. Jungclaus¹

¹Ocean in the Earth System Department, Max Planck Institute for Meteorology, Hamburg, Germany, ²Department of Environmental Sciences, Informatics and Statistics, University of Venice, Venice, Italy, ³Centre for Atmospheric Science, University of Cambridge, Cambridge, UK, ⁴Geophysical Institute, University of Bergen, Bergen, Norway, ⁵Bjerknes Centre for Climate Research, Bergen, Norway

Abstract North Atlantic sea surface temperature anomalies are known to affect tropical Pacific climate variability and El Niño–Southern Oscillation (ENSO) through thermocline adjustment in the equatorial Pacific Ocean. Here coupled climate simulations featuring repeated idealized cycles of the Atlantic Multidecadal Oscillation (AMO) generated by nudging its tropical branch demonstrate that the tropical Pacific response to the AMO also entails a substantial decadal delayed component. The simulations robustly show multidecadal fluctuations in central equatorial Pacific sea surface temperatures lagging the AMO by about three decades and a subdecadal cold-to-warm transition of the tropical Pacific mean state during the AMO's cooling phase. The interplay between out-of-phase responses of seawater temperature and salinity in the western Pacific and associated density anomalies in local thermocline waters emerge as crucial factors of remotely driven multidecadal variations of the equatorial Pacific climate. The delayed AMO influences on tropical Pacific dynamics could help understanding past and future ENSO variability.

1. Introduction

The El Niño–Southern Oscillation (ENSO) describes recurrent interannual climatic fluctuations in the equatorial Pacific that develop due to growing local instabilities of the coupled ocean-atmosphere system [*Philander, 1990*—the so-called Bjerknes feedback [*Bjerknes, 1969*—and decay due to adjustment processes of the subsurface ocean [*Neelin et al., 1998*]. Several theoretical models have been proposed to interpret ENSO dynamics and general aspects of its variability. Classical theories of ENSO ascribe a key role to the ocean thermal structure in the tropical Pacific and the associated adjustments of the equatorial thermocline [*Wang and Picaut, 2004*]. Hence, the tropical Pacific mean state crucially influences ENSO characteristics.

Most studies regard ENSO dynamics from a perspective internal to the Pacific, but a number of investigations has explored the possibility that remote forcing contributes to shaping ENSO variability. The alteration of the tropical Pacific mean state is a common key step in proposed mechanisms for multidecadal Atlantic influences on ENSO: *Timmermann et al. [2005]* describe how a collapse of the Atlantic thermohaline circulation suppresses ENSO by deepening the equatorial thermocline and reducing the vertical stratification in the equatorial Pacific Ocean; this is mostly mediated by oceanic global processes. According to *Dong and Sutton [2007]*, however, weakening of the Atlantic thermohaline circulation, which is associated with a cross-equatorial dipole in tropical Atlantic sea surface temperatures (SSTs), increases variance and induces positive skewness in ENSO; this is due to a meridionally asymmetric mean state change in the eastern equatorial Pacific triggered by atmospheric bridges and local coupled air-sea feedbacks. *Kucharski et al. [2011]* show a La Niña-like response to homogeneous anomalously warm tropical Atlantic SSTs due to easterly surface wind anomalies in the central west Pacific as part of an altered Walker circulation, whose signal is then locally amplified by coupled ocean-atmosphere processes. *McGregor et al. [2014]* propose a similar mechanism relating enhanced Atlantic warming, transbasin displacement of the main atmospheric pressure centers in the Pacific and Atlantic oceans and eastern Pacific cooling since the early 1990s.

Furthermore, *Dima et al. [2014]* link observed changes in ENSO properties since the 1970s to the great salinity anomaly in the North Atlantic via an extratropical atmospheric bridge triggered by the SST dipole which developed south of Greenland in conjunction with the freshwater anomaly. An atmospheric bridge involving intensification of the subtropical Pacific High caused by the change of phase in the Atlantic Multidecadal Oscillation (AMO) is one explanation for the recent shift from more canonical to more Central Pacific El Niños

as a Pacific Ocean response to the AMO [Yu *et al.*, 2014]. Martin-Rey *et al.* [2015] demonstrated that the strength of the Atlantic-Pacific connection and hence the contribution of tropical Atlantic SSTs to seasonal-to-interannual ENSO predictability change on multidecadal time scales.

Salinity is another factor in ENSO dynamics. Salinity influences the horizontal pressure gradients, stratification, and the equatorial thermocline [Maes *et al.*, 2005; Zheng and Zhang, 2012]. Thereby it exerts a significant modulation on the development of ENSO events. In the western Pacific warm pool salinity is thought to passively respond to ENSO-driven changes in the advective zonal fluxes of freshwater anomalies [Picaut *et al.*, 1996]. Variability of these fluxes in turn reflects changes in local precipitation, hence in upstream SSTs, atmospheric moisture advection and atmospheric stability through the position of the upwelling and downwelling branches of the Walker Cell. Salinity in the western Pacific warm pool can actively influence the precondition of major El Niño events [Maes *et al.*, 2005] and the seasonal evolution of ENSO [Zhu *et al.*, 2014]. However, the role of salinity in modulating the Pacific response to remote forcing remains largely unexplored on longer time scales.

Here we assess whether there is a robust teleconnection between AMO and tropical Pacific climate over multidecadal time scales and whether Atlantic-driven Pacific variability entails delayed responses. To this purpose, we impose idealized AMO oscillations through pattern nudging (section 2.1) in climate simulations. Our simulations describe the transient behavior of the global climate throughout the AMO cycle, including nonlinear responses of tropical Pacific to AMO on multidecadal time scales. Our approach represents a step forward compared to water hosing experiments and experiments using constant forcing associated to warm and cold AMO phases. We focus on climate model simulations since observational records incorporate externally forced signals and are too short and too noisy to individuate climatic pathways like the one we propose. We explore different amplitudes of AMO oscillations, including amplitudes comparable to instrumental observations, and twice and four times of these amplitudes in order to obtain high signal-to-noise ratios.

2. Methods

2.1. Climate Model and Pattern Nudging

The Max Planck Institute Earth system model for paleo-applications (MPI-ESM-P) [Jungclaus *et al.*, 2014] is based on the atmospheric general circulation model ECHAM6 [Stevens *et al.*, 2013] in its T63L47 configuration and the ocean-sea ice model MPIOM [Jungclaus *et al.*, 2013] in its GR15L40 configuration. The AMO characteristics simulated by MPI-ESM-P under unperturbed and under naturally forced preindustrial conditions are described by Zanchettin *et al.* [2014]. MPI-ESM realistically simulates the shape and amplitude of the ENSO power spectrum, although underestimation of the Bjerknes feedback and too low thermal damping effect degrade simulated ENSO physics [Jungclaus *et al.*, 2013].

Seventy year long AMO oscillations are imposed via pattern nudging. In our implementation, pattern nudging introduces a factor in the nudging term, providing spatially varying weights $\Omega \in [0, 1]$ to the damping time parameter τ . The nudging scheme in MPIOM accordingly takes the form

$$V_{i,j,k,t} = V_{i,j,k,t} + dt \tau \Omega_{i,j,k} (V^*_{i,j,k,t} - V_{i,j,k,t}) \quad (1)$$

where V is the 3-D field computed at time t , dt is the integration time step, and V^* is the target field. τ is set equal to $1.15e-5$.

Ω represents a pattern of oceanic or coupled atmosphere-ocean variability. Here Ω_{ij} consists of the absolute values of local correlation coefficients between the annual-mean SSTs and the spatially averaged North Atlantic SSTs (i.e., the AMO) calculated for the full length of the MPI-ESM-P preindustrial simulation (PiControl) which contributed to the fifth Coupled Model Intercomparison Project. Ω values are then imposed to be zero outside the North Atlantic, with a progressive dampening between the 50–60°N and 5°S–5°N regions to avoid the generation of artificial fronts at the borders of the nudging domain. Nudging is stronger where the correlation of the AMO with SSTs is stronger, like in the tropical branch of the AMO (inset of Figure 1a), while regions less (or not) affected by the AMO like the North Atlantic storm track region remain free to evolve fully physically consistent. The so-obtained Ω_{ij} is used for the first ocean level, and the matrix is expanded along the third, vertical dimension with a linear decrease in dampening anomalies away from the surface, so that $\Omega_{i,j,14}$ is equal to zero for all grid points. The 14th z level corresponds to a depth of 262.5 m.

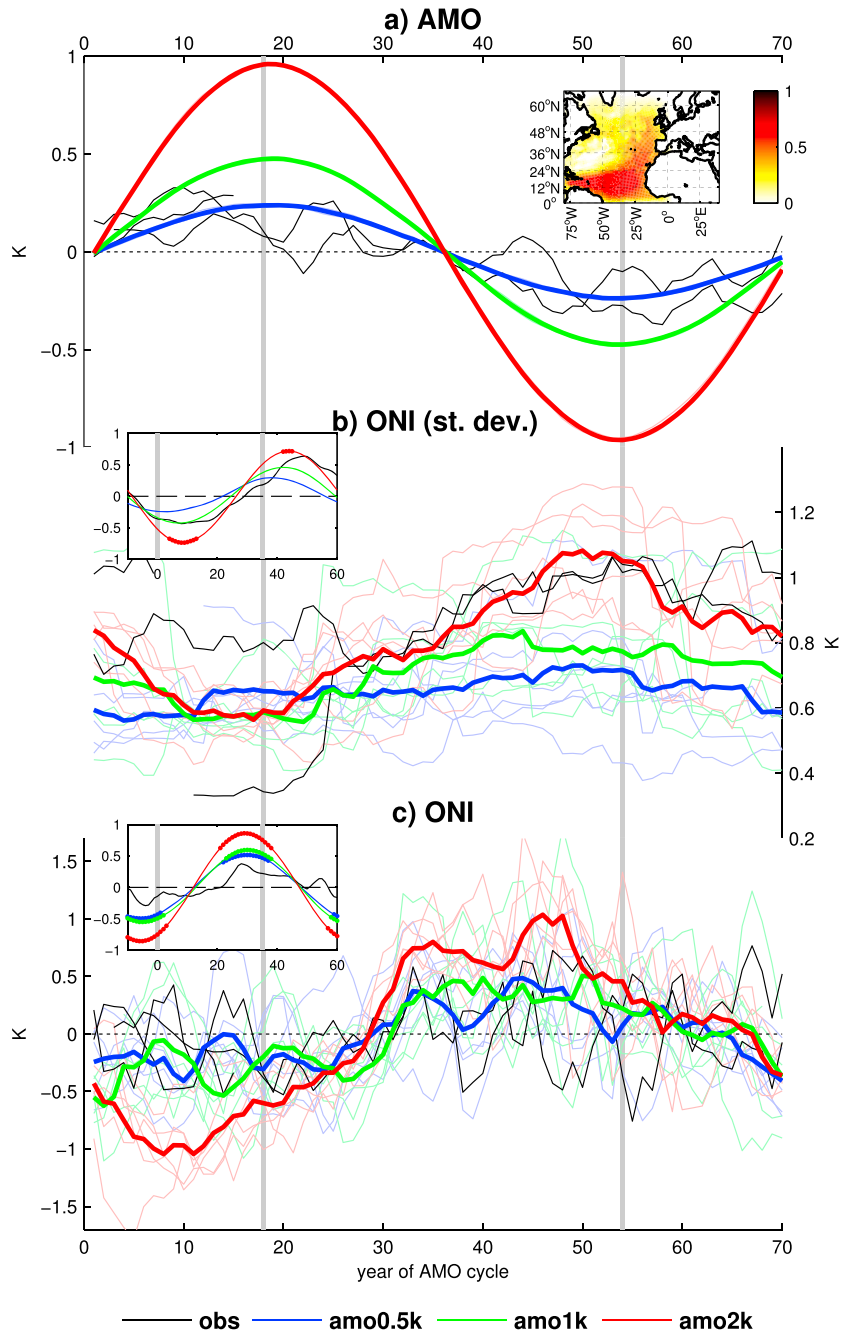


Figure 1. Changes in the tropical Pacific through the AMO cycle. Main panels: (a) evolution of AMO index, (b) ONI standard deviation over sequential 20 year periods, and (c) ONI during AMO oscillations in observations (black) and nudged simulations (colors, thin lines: individual cycles, thick lines: average cycle). The inset in Figure 1a maps the applied nudging weights. Insets in Figures 1b and 1c are the corresponding cross correlations with the AMO index, which leads by the years reported in the x axis; circles mark statistically significant values. The grey vertical lines mark the approximate occurrence of AMO's warmest and coldest state. Data were smoothed with a 5 year running mean low-pass filter.

In this application, V is the potential temperature field. The target field V^* is generated at every integration year y according to the following equation:

$$V^*_{ij,k,t} = V^C_{ij,k,t} + s \delta_y \quad (2)$$

where V^C describes the daily interpolated local monthly mean climatology calculated from PiControl, t is the day of the year, and δ_y is the value at step y of the sinusoid $\sin(2\pi y/70)$ scaled by the factor s .

2.2. Data Sets

Three simulations are conducted, each covering six successive 70 year long oscillations and all initiated from the same PiControl restart files. The three simulations differ for the amplitude of the imposed oscillations: amo0.5k describes AMO oscillations with maximum amplitudes of about 0.5 K, which is comparable to the observed amplitude of AMO fluctuations in the twentieth century and to the strongest fluctuations sporadically detected in PiControl; amo1k and amo2k describe AMO oscillations with amplitudes of about 1 K and of about 2 K, respectively.

The resulting AMO pattern extends basinwide in the North Atlantic with similar features across the nudged simulations (Figure S1 in the supporting information). The simulations display overall interannual spectral amplitudes of ENSO parameters that are comparable to observations and to PiControl, except for SST variance in the NINO1.2 region, which is substantially weaker in the model compared to observations (not shown).

Observed SST-based indices are calculated from the Extended Reconstructed Sea Surface Temperature (ERSST) v3b data set [Xue *et al.*, 2003]. The ERSSTv3b data set consists of global monthly SST analysis derived from the International Comprehensive Ocean–Atmosphere Data set with missing data filled in by statistical methods. The monthly analysis begins in January 1854.

2.3. Diagnostics

The monthly AMO index is calculated as the spatially averaged monthly mean SST over the North Atlantic (80 W–0; 0–60 N) as in Zhang and Delworth [2007] but excluding regions strongly affected by sea-ice variability [Zanchettin *et al.*, 2013, 2014]. The Oceanic Niño Index (ONI) of ENSO activity is defined as the 3 month running mean of the monthly NINO3.4 index.

Thermocline, halocline, and pycnocline are defined as the depth where the local vertical gradients of 1 m vertically (spline) interpolated potential temperature, salinity, and potential density data are maximum negative, positive, and positive, respectively. The buoyancy Brunt-Väisälä frequency squared (N^2) is calculated using the Gibbs SeaWater Oceanographic Toolbox of TEOS-10 available from <http://www.TEOS-10.org>.

Autocorrelation is taken into account in the calculation of significance of cross correlations by considering the effective degrees of freedom in both series. Data are always linearly detrended before calculating correlations. Significance of anomalies is based on an empirical estimate of the likelihood of random occurrence of the signal within the simulations following Graf and Zanchettin [2012].

Monthly ocean vertical heat transports are calculated for the mixed layer in the NINO4 region based on monthly average quantities. Heat gain and losses due to vertical advection across the mixed layer bottom are determined based on the direction of the mass transport with respect to the box: downward (i.e., outflow) transports determine heat loss by the mixed layer if the potential temperature of the local in-box grid cell is warmer than the average potential temperature of the box. The adjusted surface energy flux is the areal integral over the NINO4 region of radiative surface fluxes (long wave plus short wave) and sensible and latent heat surface fluxes, minus the downward short-wave flux at the bottom of the mixed layer. The top (bottom) surface of the grid-cell containing the mixed layer depth is used as reference for the calculation of vertical heat advection (short-wave flux) across the mixed layer.

3. Results

Our simulations show two distinct tropical Pacific responses to Atlantic SST forcing. The first relates to AMO-driven modulation of interannual-to-decadal ENSO variability depicted by recurrent increase of ONI variance during the AMO cold phase (Figures 1a, 1b, S2, and S3). The second relates to multidecadal changes in the mean state of central equatorial Pacific depicted by the ONI time series robustly lagging AMO signals by about 27 years (Figures 1a, 1c, and S3).

The first response, i.e., the inverse correlation between AMO and ENSO variance, is consistent with observations (Figure 1b) and we interpret it following the “atmospheric bridge-thermocline feedback.” In brief, westward shift of the Walker circulation cell during the warm AMO phase is associated to anomalously strong trade winds across the central and western equatorial Pacific (Figures 2b, 2d, and S4). Note that velocity potential anomalies are proportional to convergence, so negative anomalies in Figures 2d correspond to anomalous upward motion and vice versa. The anomalous winds cause thermocline deepening in the

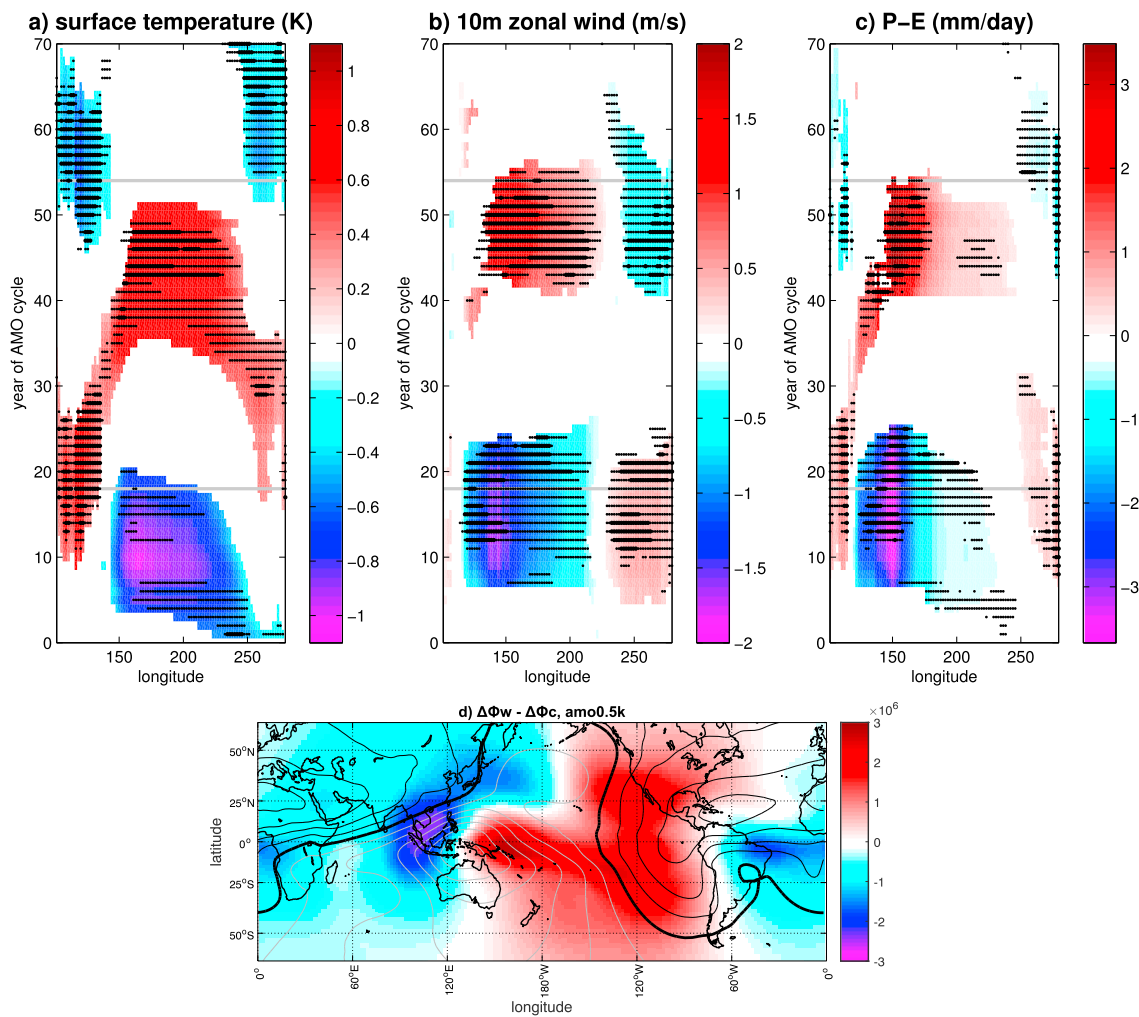


Figure 2. Average evolution of annual-mean equatorial (averaged over 5°S–5°N) Pacific anomalies of (a) surface temperature, (b) 10 m zonal wind (positive anomalies indicate eastward flow), and (c) precipitation minus evaporation through the AMO cycle. Shadings are statistically significant anomalies for the amo2k simulation; big (small) black dots indicate where anomalies are significant in all (two of) the AMO simulations. Data were smoothed with an 11 year running mean low-pass filter. The grey horizontal lines mark the approximate occurrence of AMO’s warmest and coldest state. Significance is based on 5–95 percentile range. (d) Change in the difference between winter (December–February, DJF) velocity potential at 200 hPa and 850 hPa ($\Delta\Phi$) under warm (years 7–27 of the AMO cycle) and cold (years 44–64 of the AMO cycle) AMO phases for the amo0.5k simulation. Contours are the corresponding climatology (black are positive values, grey are negative values, thick black is zero; contours are plotted at $4 \cdot 10^6 \text{ m}^2/\text{s}$ intervals).

NINO4 region, just east of the western Pacific warm pool (Figure 3a). This weakens the coupled instability through which El Niño events grow [Zebiak and Cane, 1987], hence reducing ENSO variance [Dong et al., 2006; Sutton and Hodson, 2007; Dong and Sutton, 2007]. Halocline and pycnocline in the NINO4 region deepen as well during the warm AMO phase (Figures 3b, 3c, S5, and S6), clearly describing a fast and linear response of the western equatorial Pacific to the AMO.

The multidecadal response includes a cold central and western tropical Pacific under AMO warming (Figures 3a, S5, and S6) resembling the La Niña-like response described by Kucharski et al. [2011]. Our explanation of its mechanism follows, in part, the equatorial ocean recharge paradigm described by Jin [1997]: during the warm AMO phase, the mixed layer deepens in the western equatorial Pacific and strongly gains heat via strengthened surface energy import (Figure 4) in association with the easterly wind anomaly (Figure 2b). This is consistent with the tropical Pacific Ocean being, at this stage, in a slow recharging phase. Strengthened vertical mixing and vertical mass transport, favored by decreased stability of the upper ocean layers (Figure 3), contribute to net downward energy export to subthermocline waters (Figures 4 and S7–S9). Meanwhile, positive salinity anomalies develop (Figure 3b) due to the significantly weakened atmospheric

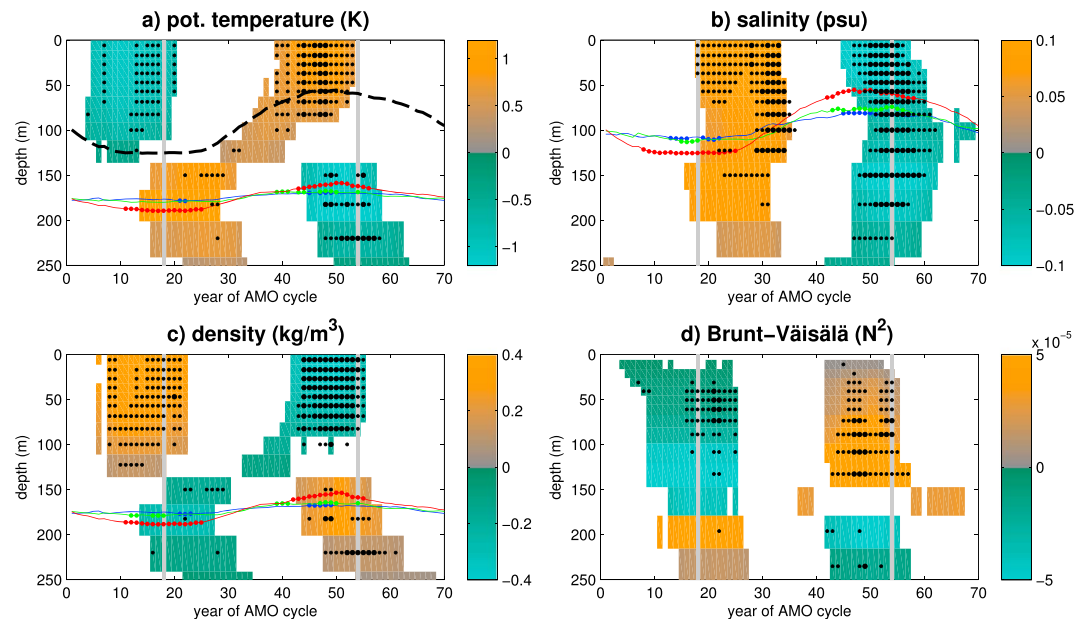


Figure 3. Average evolution of winter (DJF) oceanic properties in the NINO4 region through the AMO cycle. Anomalies of (a) potential temperature, (b) salinity, (c) density, and (d) Brunt-Väisälä frequency squared (N^2) are calculated from each level's climatology. Shadings are statistically significant anomalies for the amo2k simulation; big (small) black dots indicate where anomalies are significant in all (two of) the AMO simulations. Line plots in Figures 3a–3c are the evolutions of thermocline (Figure 3a), halocline (Figure 3b), and pycnocline (Figure 3c) depth (color code for simulations as for Figure 1); dots mark significant anomalies. The thick black dashed line in Figure 3a is the halocline for simulation amo2k. Data were smoothed with an 11 year running mean low-pass filter. The grey vertical lines mark the approximate occurrence of AMO's warmest and coldest state. Significance is based on 5–95 percentile range.

convective activity over the western tropical Pacific (Figures 2d and S4) and, hence, of the reduced precipitation that dominates the local anomalous precipitation-evaporation flux (Figures 2c and S10). The so-established saltier water column during and after the AMO warm phase (Figure 3b, years ~20–30) maintains stably stratified conditions at thermocline and subthermocline depths (at and below 200 m; see Figure 3d) by counteracting the destabilizing effect of locally warmer potential temperatures (Figure 3a). The resulting thermocline cooling/subthermocline warming at this stage (Figure 3) is therefore strongly related to changes in oceanic transport (Figures 4a–4c).

Then, about 10–15 years after the AMO warm peak, the tropical Pacific undergoes a subdecadal transition from a recharged to a discharging state. This transition is represented by the sharp drop in the mixed layer heat content in the NINO4 region (Figures 4a–4c) and by the rapid warming of SST anomalies occurring in the central Pacific around year 30 of the AMO oscillation (Figure 1c). The residuals of a least squares linear regression of ONI on the AMO index also show this component of the multidecadal cyclic behavior of the tropical Pacific (not shown), which is then linearly independent from the atmospheric-driven mechanisms introduced above. According to this regression model, the relative amplitude of decadal smoothed residuals and predicted ONI values ranges between 1.2 (amo2k) and 3.2 (amo0.5k). Hence, this feature of tropical Pacific climate accounts for changes in the mean state as important as the direct/linear response. This transition period is also characterized, in all simulations, by a westward migration of maximum annual-average SST anomalies along the equatorial Pacific (Figure S11).

The drop in mixed layer heat content is related to reduced import through surface fluxes (Figures 4d–4f), especially a sharp increase in latent heat losses (Figure S10), and to volume loss due to thermocline/pycnocline rise. However, a steep increase in the mixed layer average temperature occurs due to a concomitant sharp drop in the mixed layer heat losses due to vertical advection (Figure 4). Buoyancy changes are again involved in this process: the amo2k simulation clearly shows an apparent upwelling of positive potential temperature anomalies, with the deep portion of the mixed layer, below the halocline, warming first and the halocline representing an upper boundary for the upwelling of the warm anomalies (Figure 3a). We therefore surmise that the weakening of

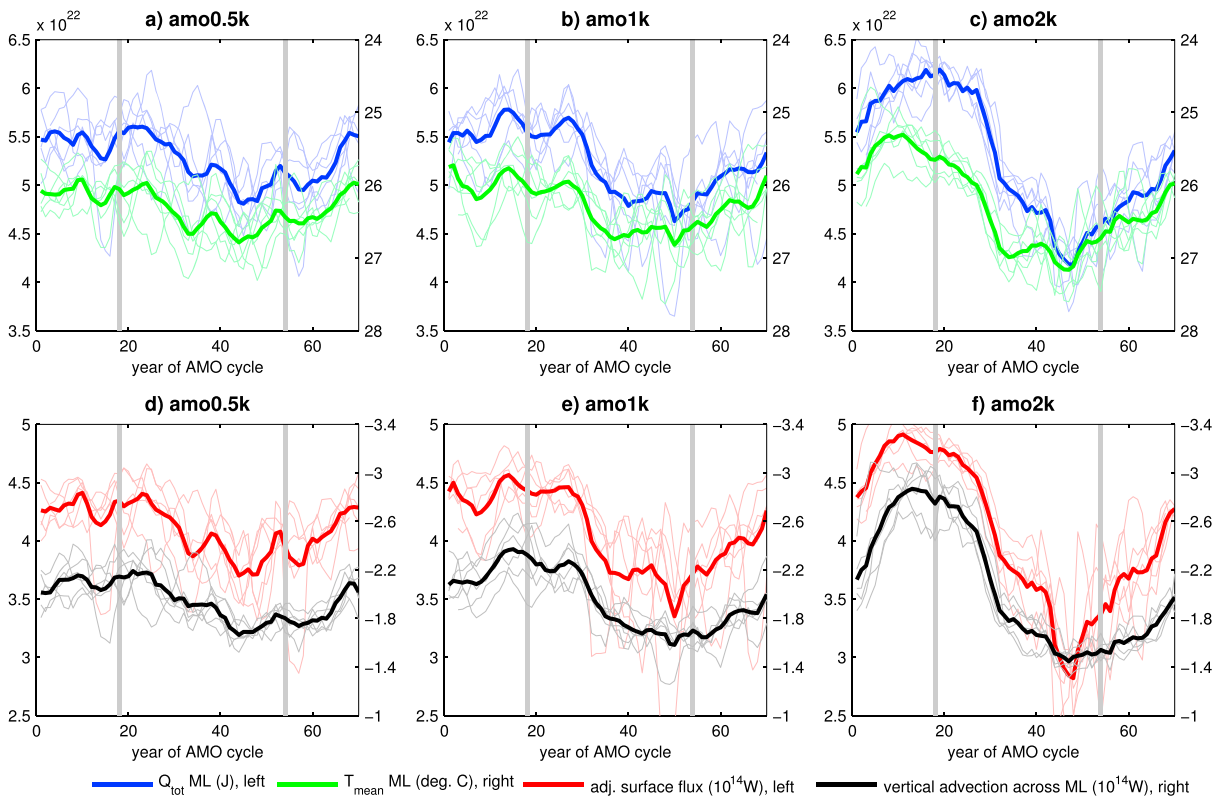


Figure 4. Ocean heat changes in the NINO4 region. (a–c) Heat content and average potential temperature for the mixed layer. (d–f) Adjusted surface heat flux and downward heat transport by vertical advection across the mixed layer boundary. Positive transport values correspond to heat gain by the mixed layer and vice versa.

positive salinity anomalies after year 30 of the AMO oscillation is associated with a rapid deterioration of the stable subthermocline conditions (Figure 3) that temporarily enhances the atmospheric-driven discharge process. Accordingly, the evolution of oceanic properties in the western and central Pacific—specifically the out-of-phase evolution of upper ocean potential temperature and salinity anomalies (Figures 3a, 3b, S5, and S6)—appears as a key factor contributing to the abovementioned nonlinear response of the tropical Pacific to the AMO.

The nonlinearity is not detected during the warming phase of the AMO cycle, around years 55–70 and 1–15 of the AMO oscillation, when positive subthermocline density anomalies in the western Pacific warm pool determine unstable local stratification (Figure 3c). The mechanism therefore provides asymmetry in the response of the tropical Pacific to opposite AMO phases.

4. Summarizing Discussion

Our simulations show an out-of-phase response of the tropical Pacific to the AMO on multidecadal time scales. We also ascribe a subdecadal transition of the tropical Pacific mean state during the AMO cooling phase to changes in ocean stratification and in particular to salinity in the western and central tropical Pacific that temporarily enhance a slower atmospheric-driven discharge process in the equatorial Pacific Ocean. Our results add to formerly suggested pathways for decadal-scale responses of Pacific climate to Atlantic multidecadal variability [e.g., Timmermann *et al.*, 2005; Dong and Sutton, 2007; Zhang and Delworth, 2007; D’Orgeville and Peltier, 2007]. Seawater salinity and remote forcing are commonly considered as factors of second-order importance for present-day interannual ENSO dynamics and variability; our study highlights how they can become determinant contributors on multidecadal timescales. Additionally, our simulations demonstrate that AMO patterns with a basinwide signature in the North Atlantic can be generated by nudging only the tropical branch of the AMO.

Our dynamical interpretation for the Atlantic-Pacific connection omits the role of global oceanic processes like the global baroclinic ocean adjustment [Timmermann *et al.*, 2005]. Our nudging procedure results in an

inverse correlation between AMO and strength of the Atlantic thermohaline circulation (not shown). This contrasts the typical relation found in unperturbed simulations with MPI-ESM [e.g., Zanchettin *et al.*, 2014, 2015] where the AMO represents a surface signature of the overturning circulation rather than a forcing factor as in our nudging simulations. It is unclear how this behavior affects the overall thermocline response. We note, anyway, that recent work has questioned the relevance of the oceanic overturning circulation as driver of the AMO [Clement *et al.*, 2015]. Long-term drifts in regional and global temperature and salinity in the deeper ocean layers represent a further caveat to our results (Figure S12). Drifts, however, do not affect noticeably the upper ocean layers that are focus of this study.

The interpretation also neglects the role of extratropical atmospheric bridges [e.g., Zhang and Delworth, 2007] and more generally of the large-scale tropospheric circulation. We indeed diagnose multidecadal signals in the Aleutian low region and Arctic sea ice (Figure S13), but these are overall less robust than the tropical signals. This could be due to the tropical signature of the imposed nudging (Figure 1a). Extratropical implications for the tropical response, especially concerning the freshwater fluxes, are left to a follow-up study.

The realism of the mechanism described above mainly relies on two facts: the realism of our simulations and observational support for the mechanism. Ocean properties and variability in MPI-ESM are affected by known regional biases in both temperature and salinity [Jungclaus *et al.*, 2013]. These may enhance or dampen key processes described here and especially the buoyancy response. Quantifying the effects of such biases is difficult, especially since model biases depend on the mean climate state [Kerckhoff *et al.*, 2014] and the latter substantially varies in our simulations.

Zanchettin *et al.* [2015] recently demonstrated that Pacific-Atlantic SST interactions in an ensemble of unperturbed climate simulations vary on interdecadal and multidecadal time scales so that different mechanisms being active during different periods can lead to lack of robust interbasin signals. The results described here do not necessarily contradict this statement: first, the nudging as performed here highlights the tropical branch of the AMO pattern, and then, AMO fluctuations with amplitude comparable to that in amo0.5k occur only sporadically in an unperturbed millennial simulation with MPI-ESM-P, so that the lack of robust multidecadal interbasin signals may be due to a low signal-to-noise ratio as discussed in Zanchettin *et al.* [2015].

There are some discrepancies between simulated behavior and the observational record (Figure 1). This does not necessarily imply that our mechanism is a model artifact: The mechanism may well have not been detectable during the late nineteenth and twentieth century due to the substantial external disturbances of the climate system. Note that the detrended observed evolutions in Figure 1 (black line) only partly reflect changes related to, e.g., changing background conditions of the tropical Pacific due to global warming and volcanic effects on both ENSO [Li *et al.*, 2011] and the AMO [Zanchettin *et al.*, 2012, 2013]. Furthermore, the observed AMO evolution entails substantial interannual variability, which further hampers the detection of any AMO-driven multidecadal signal in remote regions; in contrast, interannual variability over the Atlantic is strongly damped in our simulations by the nudging process (Figure 1a). The oceanic part of the described mechanism is similarly less significant in the amo0.5k simulation, with significance arguably increasing with the number of simulated AMO cycles. Therefore, shortness of the observational record and a low signal-to-noise ratio are plausible explanations for the lack of detectability of this mechanism in observations.

Active/latent phases of the mechanism can substantially affect decadal variability in the tropics. Thereby our results call for continued seawater monitoring in the western tropical Pacific [Tollefson, 2014] and highlights possible long-term benefits of an improved observing system there [Gasparin *et al.*, 2015]. They also highlight the need for improved salinity initialization in decadal climate prediction experiments. Further, the mechanism is relevant for climate model evaluation, particularly concerning remote impacts of model biases originating in the tropical Atlantic Ocean. Lastly, reliability of regional climate predictability assessments may depend on earth system model and assimilation systems capturing the described link between the AMO and the equatorial Pacific.

Acknowledgments

This work was funded by the Bundesministerium für Bildung und Forschung (BMBF) research program "MiKlip" (FKZ:01LP1158A) and by the European project PREFACE (603521). D.Z. thanks the Max Planck Institute for Meteorology for providing him support as visiting scientist. Ralf Hand provided useful comments that helped improve the quality of the manuscript. We also thank two anonymous reviewers for their constructive criticism. Primary data and scripts used in the analysis and other supporting information that may be useful in reproducing the author's work are archived by the Max Planck Institute for Meteorology and can be obtained by contacting publications@mpimet.mpg.de

References

- Bjerknes, J. (1969), Atmospheric teleconnections from the equatorial Pacific, *Mon. Weather Rev.*, *97*, 163–172.
- Clement, A., K. Bellomo, L. N. Murphy, M. A. Cane, T. Mauritsen, G. Rädel, and B. Stevens (2015), The Atlantic Multidecadal Oscillation without a role for ocean circulation, *Science*, *350*(6258), 320–324.
- Dima, M., G. Lohmann, and N. Rambu (2014), Possible North Atlantic origin for changes in ENSO properties during the 1970s, *Clim. Dyn.*, doi:10.1007/s00382-014-2173-x.

- Dong, B., and R. T. Sutton (2007), Enhancement of ENSO variability by a weakened Atlantic thermohaline circulation in a coupled GCM, *J. Clim.*, *20*, 4920–4939.
- Dong, B., R. T. Sutton, and A. A. Scaife (2006), Multidecadal modulation of El Niño–Southern Oscillation (ENSO) variance by Atlantic Ocean sea surface temperatures, *Geophys. Res. Lett.*, *33*, L08705, doi:10.1029/2006GL025766.
- D'Orgeville, M., and W. R. Peltier (2007), On the Pacific Decadal Oscillation and the Atlantic Multidecadal Oscillation: Might they be related?, *Geophys. Res. Lett.*, *34*, L23705, doi:10.1029/2007GL031584.
- Gasparin, F., D. Roemmich, J. Gilson, and B. Cornuelle (2015), Assessment of the upper-ocean observing system in the equatorial Pacific: The role of Argo in resolving intraseasonal to interannual variability, *J. Atmos. Oceanic Technol.*, *32*, 1668–1688, doi:10.1175/JTECH-D-14-00218.1.
- Graf, H. F., and D. Zanchettin (2012), Central Pacific El Niño, the “subtropical bridge” and Eurasian climate, *J. Geophys. Res.*, *117*, D01102, doi:10.1029/2011JD016493.
- Jin, F.-F. (1997), An equatorial ocean recharge paradigm for ENSO. Part I: Conceptual model, *J. Atmos. Sci.*, *54*, 811–829.
- Jungclaus, J. H., N. Fischer, H. Haak, K. Lohmann, J. Marotzke, D. Matei, U. Mikolajewicz, D. Notz, and J. S. von Storch (2013), Characteristics of the ocean simulations in MPIOM, the ocean component of the Max Planck Institute Earth System Model, *J. Adv. Model. Earth Syst.*, *5*, 422–446, doi:10.1002/jame.20023.
- Jungclaus, J. H., K. Lohmann, and D. Zanchettin (2014), Enhanced 20th-century heat transfer to the Arctic simulated in the context of climate variations over the last millennium, *Clim. Past*, *10*, 2201–2213, doi:10.5194/cp-10-2201-2014.
- Kerkhoff, C., H. R. Künsch, and C. Schär (2014), Assessment of bias assumptions for climate models, *J. Clim.*, *27*, 6799–6818.
- Kucharski, F., I.-S. Kang, R. Farneti, and L. Feudale (2011), Tropical Pacific response to 20th century Atlantic warming, *Geophys. Res. Lett.*, *38*, L03702, doi:10.1029/2010GL046248.
- Li, J., S.-P. Xie, E. R. Cook, G. Huang, R. D'Arrigo, F. Liu, J. Ma, and X.-T. Zheng (2011), Interdecadal modulation of El Niño amplitude during the past millennium, *Nat. Clim. Change*, *1*(2), 114–118, doi:10.1038/nclimate1086.
- Maes, C., J. Picaut, and S. Belamari (2005), Importance of salinity barrier layer for the buildup of El Niño, *J. Clim.*, *18*, 104–118.
- Martín-Rey, M., B. Rodríguez-Fonseca, and I. Polo (2015), Atlantic opportunities for ENSO prediction, *Geophys. Res. Lett.*, *42*, 6802–6810, doi:10.1002/2015GL065062.
- McGregor, S., A. Timmermann, M. F. Stuecker, M. H. England, M. Merrifield, F.-F. Jin, and Y. Chikamoto (2014), Recent Walker circulation strengthening and Pacific cooling amplified by Atlantic warming, *Nat. Clim. Change*, *4*, 888–892, doi:10.1038/nclimate2330.
- Neelin, J., D. Battisti, A. Hirst, F. Jin, Y. Wakata, T. Yamagata, and S. Zebiak (1998), ENSO theory, *J. Geophys. Res.*, *103*, 14,261–14,290, doi:10.1029/97JC03424.
- Philander, S. G. H. (1990), *El Niño, La Niña and the Southern Oscillation*, Academic, London.
- Picaut, J., M. Ioualalen, C. Menkes, T. Delcroix, and M. McPhaden (1996), Mechanism of the zonal displacements of the Pacific warm pool, implications for ENSO, *Science*, *274*, 1486–1489.
- Stevens, B., et al. (2013), Atmospheric component of the MPI-M Earth system Model: Echem6, *J. Adv. Model. Earth Syst.*, *5*, 146–172, doi:10.1002/jame.20015.
- Sutton, R., and D. Hodson (2007), Climate response to basin-scale warming and cooling of the North Atlantic Ocean, *J. Clim.*, *20*(5), 891–907, doi:10.1175/JCLI4038.1.
- Timmermann, A., S.-I. An, U. Krebs, and H. Goosse (2005), ENSO suppression due to weakening of the North Atlantic thermohaline circulation, *J. Clim.*, *18*, 3122–3139.
- Tollefson, J. (2014), El Niño monitoring system in failure mode, *Nature*, doi:10.1038/nature.2014.14582.
- Wang, C., and J. Picaut (2004), Understanding ENSO physics—A review, in *Earth's Climate: The Ocean-Atmosphere Interaction*, *Geophys. Monogr.*, vol. 147, pp. 21–48, AGU, Washington, D. C., doi:10.1029/147GM02.
- Xue, Y., T. M. Smith, and R. W. Reynolds (2003), Interdecadal changes of 30-yr SST normals during 1871–2000, *J. Clim.*, *16*, 1601–1612.
- Yu, J., P. Kao, H. Paek, H. Hsu, C. Hung, M. Lu, and S. An (2014), Linking emergence of the Central-Pacific El Niño to the Atlantic multi-decadal oscillation, *J. Clim.*, *28*, 651–662, doi:10.1175/JCLI-D-14-00347.1.
- Zanchettin, D., C. Timmreck, H.-F. Graf, A. Rubino, S. Lorenz, K. Lohmann, K. Krueger, and J. H. Jungclaus (2012), Bi-decadal variability excited in the coupled ocean-atmosphere system by strong tropical volcanic eruptions, *Clim. Dyn.*, *39*(1–2), 419–444, doi:10.1007/s00382-011-1167-1.
- Zanchettin, D., A. Rubino, D. Matei, O. Bothe, and J. H. Jungclaus (2013), Multidecadal-to-centennial SST variability in the MPI-ESM simulation ensemble for the last millennium, *Clim. Dyn.*, *40*(5), 1301–1318, doi:10.1007/s00382-012-1361-9.
- Zanchettin, D., O. Bothe, W. Müller, J. Bader, and J. H. Jungclaus (2014), Different flavors of the Atlantic Multidecadal Variability, *Clim. Dyn.*, *42*(1–2), 381–399, doi:10.1007/s00382-013-1669-0.
- Zanchettin, D., O. Bothe, A. Rubino, and J. H. Jungclaus (2015), Multi-model ensemble analysis of Pacific and Atlantic SST variability in unperturbed climate simulations, *Clim. Dyn.*, doi:10.1007/s00382-015-2889-2.
- Zebiak, S., and M. Cane (1987), A model El Niño–Southern Oscillation, *Mon. Weather Rev.*, *115*, 2262–2278.
- Zhang, R., and T. L. Delworth (2007), Impact of the Atlantic Multidecadal Oscillation on North Pacific climate variability, *Geophys. Res. Lett.*, *34*, L23708, doi:10.1029/2007GL031601.
- Zheng, F., and R.-H. Zhang (2012), Effects of interannual salinity variability and freshwater flux forcing on the development of the 2007/08 La Niña event diagnosed from Argo and satellite data, *Dyn. Atmos. Oceans*, *57*, 45–57.
- Zhu, J., B. Huang, R.-H. Zhang, Z.-Z. Hu, A. Kumar, M. A. Balmaseda, L. Marx, and J. L. Kinter III (2014), Salinity anomaly as a trigger for ENSO events, *Sci. Rep.*, *4*, 6821, doi:10.1038/srep06821.